Self-Organized Gels in DNA/F-Actin Mixtures without Crosslinkers: Networks of Induced Nematic Domains with Tunable Density

Ghee Hwee Lai,[1] John C. Butler,[2] Olena V. Zribi,[1] Ivan I. Smalyukh,[2,3,*] Thomas E. Angelini,[1,4] Kirstin R. Purdy,[2] Ramin Golestanian,[5] and Gerard C. L. Wong[2,1,†]

[1]*Department of Physics, University of Illinois at Urbana-Champaign, Urbana, Illinois 61801, USA*
[2]*Department of Materials Science and Engineering, University of Illinois at Urbana-Champaign, Urbana, Illinois 61801, USA*
[3]*Department of Physics, University of Colorado at Boulder, Boulder, Colorado 80309, USA*
[4]*Department of Engineering and Applied Science, Havard University, Cambridge, Massachusetts 02138, USA*
[5]*Department of Physics and Astronomy, University of Sheffield, Sheffield S3 7RH, United Kingdom*
(Received 20 September 2007; revised manuscript received 4 September 2008; published 19 November 2008)

We examine mixtures of DNA and filamentous actin (F-actin) as a model system of like-charged rigid rods and flexible chains. Confocal microscopy reveals the formation of elongated nematic F-actin domains reticulated via defect-free vertices into a network embedded in a mesh of random DNA. Synchrotron x-ray scattering results indicate that the DNA mesh squeezes the F-actin domains into a nematic state with an interactin spacing that decreases with increasing DNA concentration as $d_{\text{actin}} \propto \rho_{\text{DNA}}^{-1/2}$. Interestingly, the system changes from a counterion-controlled regime to a depletion-controlled regime with added salt, with drastic consequences for the osmotic pressure induced phase behavior.

PACS numbers: 82.35.Rs, 61.30.−v, 87.14.gk

Interactions between flexible chains and rigid rods govern a broad range of systems, including liquid crystalline (LC) polymers [1,2], polymer-nanotube fibers [3], composite metamaterials [4], and biological tissues [5–7], and may be relevant for DNA oligomers purification [8]. Flory theory predicts the coexistence of isotropic and anisotropic phases from the existence of dissimilar flexibility [9], which have been confirmed in polymeric mixtures with different persistence lengths [10–12]. However, polymer systems with a hierarchy of interactions can exhibit surprising behavior [13–16]. It is not known how the existence of strong electrostatic interactions modifies the basic Flory behavior of phase separation in composite systems, nor if any additional forms of self-organization occur.

In this Letter, we study the phase behavior in semidilute mixtures of like-charged actin rods and DNA chains using confocal microscopy and synchrotron x-ray diffraction. Instead of macroscopic phase separation, we find an entangled percolating network of elongated nematic filamentous actin (F-actin) domains threading through a mesh of random DNA coils. The more highly charged DNA coils compress F-actin rods and induce nematic order at concentrations well below the Onsager criterion [17]. The interactin molecular spacing in these nematic domains exhibits a power-law dependence on DNA concentration $d_{\text{actin}} \propto \rho_{\text{DNA}}^{-1/2}$, consistent with the mechanical balance of counterion-dominated osmotic pressure between phase-separated domains. With added salt, the system undergoes a transition from a ''strongly charged'' regime dominated by counterion-controlled osmotic pressure to a ''weakly charged'' regime dominated by conventional depletion effects. The entire phenomenon is entropic in origin. Interestingly, by restructuring perpendicular crossings into locally tangent crossings, these nematic domains are reticulated into a network without forming bulk defects, suggesting that mixtures of biopolymers with different flexibilities may lead to unexpected mechanical properties.

DNA molecules (diameter $D_{\text{DNA}} = 2$ nm, charge density $e^-/0.17$ nm, persistence length $\lambda_{\text{DNA}} = 50$ nm) of two different contour lengths (48 and 10 kbp) were ethanol precipitated and resuspended in deionized water to specific concentrations. Lyophilized rabbit skeletal muscle globular actin (G-actin), molecular weight (MW) 43 000, was suspended in a pH 8 buffer (5 mM Tris, 0.2 mM CaCl$_2$, 0.5 mM ATP, 0.2 mM DTT, 0.01% NaN$_3$) and polymerized to F-actin in 100 mM KCl and phalloidinated ($D_{\text{actin}} = 7.5$ nm, charge density $e^-/0.25$ nm, $\lambda_{\text{actin}} = 10$ μm). The average filament length $\ell_{\text{actin}} = 0.3$–$10$ μm was varied
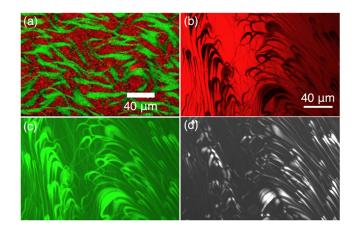

FIG. 1 (color online). (a) Fluorescence confocal image of phase-separated domains of F-actin [light gray (green)] and DNA [dark gray (red)]. Colocalized same-area fluorescence showing (b) DNA [gray (red)], (c) F-actin [white (bright green)], and (d) PM image of the birefringent F-actin domains.

using human plasma gelsolin (MW 87 000). DNA and F-actin solutions are mixed at different ratios, with the global actin concentration kept constant at 5 mg/ml.

We used a Leica TCS SP2 confocal microscope and a Nikon E200POL polarizing microscope (PM) with an oil-immersion objective ($63 \times$, numerical aperture 1.4). F-actin was dyed using Alexa Fluor 488 phalloidin or Alexa Fluor 568 phalloidin. DNA was dyed with POPO-3. Dyed and unlabeled biopolymers were mixed in a proportion of 1:100. Small angle x-ray scattering (SAXS) measurements were performed on sealed samples at the Stanford Synchroton Radiation Laboratory (BL 4-2, 10 keV incident beam, with a beam size of $300 \times 300 \ \mu\mathrm{m}^2$, coupled to a MAR Research CCD camera, pixel size 79 μm).

A representative confocal micrograph of a F-actin/DNA mixture ([DNA] = 1.14 mg/ml) is shown in Fig. 1(a) [18]. F-actin is organized into elongated domains (green, typical lengths 50–1000 μm and widths 1–20 μm) embedded in a mesh of DNA chains (red). Figures 1(b)–1(d), 2(a), and 2(b) show the same-area textures in fluorescence and PM modes. The DNA fluorescence signal does not overlap with that from F-actin, indicating local phase separation. Vertical confocal cross sections show that this phase separation is not affected by confinement or the surface affinity of either DNA or F-actin with multiple F-actin domains spanning the same thickness [Figs. 2(f)–2(h)]. Birefringent nematic domains of F-actin form an interconnected network through a nonbirefringent isotropic matrix of DNA [Figs. 1 and 2(a)–2(e)]. PM textures obtained with crossed polarizers have extinction brushes within the regions where the LC director $\hat{n}$ (average local orientation of the F-actin rods) is parallel or perpendicular to the polarizers [Fig. 2(b)]. As the sample is rotated, the dark brushes move, visualizing $\hat{n}$ [Fig. 2(c)]. Using the first-order interference colors in PM textures obtained with a 530 nm phase retardation plate inserted between the crossed polarizers, we find that $\hat{n}$ is parallel to the walls of the domains. Rods oriented parallel to the interface of F-actin and DNA domains have configurational entropy lower by $\sim k_B \ln(\ell_\mathrm{actin}/D_\mathrm{actin})$ compared to the perpendicular case [2], leading to a free energy difference of 4–$8k_BT$ per F-actin. Consistent with this, tangential surface anchoring is observed for the entire DNA concentration range studied 0.5–7.5 mg/ml and for different biopolymer lengths.

The nematic F-actin domains percolate across the sample, due to domain stiffness. There are two complementary ways in which domain formation can enhance bending rigidity: (1) the individual filaments in the larger domain resist bending collectively, (2) tilt restrictions are imparted on filaments of length ℓ_actin by the cages of width d_actin surrounding them. The first mechanism gives the Frank elastic constant $K_3 \sim k_B T \lambda_\mathrm{actin}/d_\mathrm{actin}^2$ describing bend distortions of $\hat{n}$ [19]. The second mechanism depends on ℓ_actin since the restrictions are geometric. The nematic free energy cost of a rod confined in its cage can be estimated
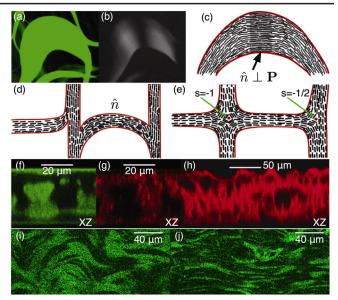

FIG. 2 (color online). Morphology and director structures in a network of nematic domains. (a) A fluorescence texture of a bent F-actin domain [gray (green)]. (b) A colocalized polarizing microscopy texture. (c) Schematics of $\hat{n}$ in the bent domain shown in (a),(b); the dark brushes show where $\hat{n}$ is parallel or perpendicular to the crossed polarizers. (d),(e) Schematics of different domain nodes: (d) formed without bulk defects in $\hat{n}$ and frequently observed, (e) containing defects and rarely observed. (f)–(h) Vertical confocal cross sections showing (f) the F-actin domains [gray (green)] and (g),(h) surrounding DNA [gray (red)]. In the colocalized images (f),(g), single phase-separated domains span across the sample. The multidomain distribution is shown in (h). As the DNA concentration increases from (i) 1 mg/ml to (j) 7.5 mg/ml, the actin domains decrease in width.

as $K_3[(d_\mathrm{actin}/\ell_\mathrm{actin})/\ell_\mathrm{actin}]^2(\ell_\mathrm{actin}d_\mathrm{actin}^2)$, which is to be balanced by k_BT. One finds $K_3 \sim k_BT\ell_\mathrm{actin}^3/d_\mathrm{actin}^4$, which is consistent with the first mechanism if we replace ℓ_actin by the Odijk deflection length ($\sim \lambda_\mathrm{actin}^{1/3}d_\mathrm{actin}^{2/3}$). For our experiments, the two formulas yield similar estimates of $K_3 = 10^{-11}$ N, as the size of actin is comparable to the Odijk length. We estimate an effective domain persistence length $\lambda_d = B/k_BT \approx K_3 h_d^2/2k_BT$, where B is the bend modulus and h_d is the lateral size of a domain. For $h_d = 1 \ \mu$m, one finds $\lambda_d = 120 \ \mu$m. The domains are significantly stiffer than individual F-actin rods, which facilitates their percolative spanning of a sample.

The nematic F-actin domains tend to self-organize into a 3D network "anchored" at confining surfaces (Fig. 2). In these 3D networks, the director $\hat{n}$ of domains forming a node smoothly transforms between the domains without forming bulk defects (Figs. 1 and 2). The angles between domains at the nodes are small, which is satisfied by domain bending [Fig. 2(d)]. When the surface boundary conditions for $\hat{n}$ at the domain walls are tangential, planar straight connection of N domains results in a defect line of strength $s = (2 - N)/2$ that runs across the domain of thickness h_d [Fig. 2(e)]. Neglecting the difference in the

values of Frank elastic constants [1], the free energy of a disclination of strength s is $\sim \pi s^2 K h_d \ln(h_d/r_{\text{core}}) + T_{\text{core}} h_d$, where K is the average Frank elastic constant, r_{core} and T_{core} are the radius and line tension of the defect core. For typical parameters [1,2], free energy associated with the defects is $\sim(60–800) \times 10^{-18}$ J, two orders of magnitude larger than the elastic free energy associated with bending of the nematic domains. Not only is this consistent with the observed defect-free morphology of these networks, this condition places strong constraints on how the elongated domains interact with each other. Nonparallel F-actin domains that come together will have to nucleate an energetically costly disclination [Fig. 2(d)], unless one or both of them can undergo a bend distortion and bring $\hat{n}$ into local alignment at the node [Fig. 2(e)]. This is analogous to an entanglement, and potentially acts as a kinetic barrier against the crossing of actin domains. Although the samples are essentially the same when re-measured a year later, it is possible that the observed organization is in a kinetically frozen nonequilibrium state.

The formation of nematic domains is not expected for these solution conditions, as the constituting F-actin and DNA aqueous solutions are both isotropic at the concentrations in question. The birefringence (Figs. 1 and 2) can be seen even at 5 mg/ml, which is well below the Onsager criterion $4.48/(\pi D_{\text{actin}} \ell_{\text{actin}}^2/4)$ for nematic order [17]. Electrostatic interactions can lead to an expanded effective diameter of F-actin rods [17] as well as twisting tendencies [20], which can modify the threshold concentration for LC order. However, our experiments give no evidence of anisotropy in aqueous solutions of the F-actin rods of $\ell_{\text{actin}} = 300$ nm at 5 mg/ml, consistent with previous studies [21]. Furthermore, we find that as the concentration of DNA is increased from 1 to 7.5 mg/ml at a constant F-actin concentration of 5 mg/ml, we do not see a coarsening to larger domain structures, as expected from an increase in the interdomain depletion attraction induced by the DNA concentration increase. Instead, a marked increase in the aspect ratios of the domains is observed [Figs. 2(i) and 2(j)], and "threadlike" nematic domains of F-actin are formed with increasing DNA concentration.

We perform SAXS experiments to elucidate the relation between DNA and the induced nematic F-actin organization (Fig. 3). The nematic F-actin subphase in a representative F-actin/DNA mixture (1.75 mg/ml DNA, 5 mg/ml F-actin) has a smaller nematic spacing than that for an aqueous actin formed at 50 mg/ml F-actin ($\sim 10\times$ higher concentration). Clearly, DNA compresses the F-actin into a dense nematic phase. To investigate this quantitatively, we varied the DNA concentration between 0.67 and 4 mg/ml at a fixed F-actin concentration of 5 mg/ml. We find that the average interactin spacing d_{actin} is controlled by the DNA concentration ρ_{DNA} via a power-law dependence $d_{\text{actin}} \propto \rho_{\text{DNA}}^{-1/2}$, which does not depend significantly on DNA length [Fig. 3(c)]. For example, the slope in a log-log plot of d_{actin} versus relative concentration is $-0.50 \pm$
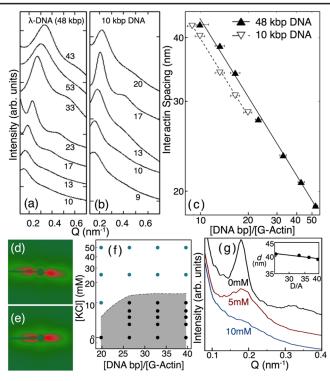

FIG. 3 (color online). Circularly averaged SAXS data for (a) 48 kbp DNA and (b) 10 kbp DNA show similar trends. The interactin spacing decreases as the concentration of DNA increases. (c) Log-log plot of the interactin spacing d_{actin} versus molar ratio of DNA bp to G-actin monomers for 48 kbp DNA (solid line) and 10 kbp DNA (dashed line); best linear fits provide slopes -0.502 ± 0.055 and -0.498 ± 0.087, respectively. (d),(e) 2D SAXS images of (d) F-actin DNA mixtures (5 mg/ml actin) and that of (e) pure F-actin (50 mg/ml actin). (f) Phase diagram of DNA F-actin mixture in KCl. The shaded area indicates induced nematic order. (g) SAXS data for DNA F-actin mixture (2.5 mg/ml DNA, 5 mg/ml F-actin) show suppression of nematic order with KCl. Inset: Log-log plot of d_{actin} at 10 mM KCl with slope -0.201 ± 0.051, which is distinct from the no-salt behavior.

0.06 for 48 kbp DNA and -0.50 ± 0.09 for 10 kbp DNA. To explain this dependence, we consider the mechanical and chemical equilibrium between the mesh of DNA chains and F-actin domains. At concentrations of 0.5–7.5 mg/ml, DNA molecules form an entangled solution of semiflexible chains with the mesh size ξ_{DNA} comparable to its persistence length λ_{DNA}. On the scale of λ_{DNA}, DNA can be viewed as rodlike molecules; therefore, the mesh size $\xi_{\text{DNA}} \propto \rho_{\text{DNA}}^{-1/2}$ shrinks with increasing concentration within the semidilute regime [22,23]. For highly charged polyelectrolytes with no added salt, the osmotic pressure of an aqueous solution is dominated by the contribution of the uncondensed counterions [24]. The osmotic pressure of free counterions in a solution of actin rods is $\Pi_{\text{actin}} \propto k_B T/\ell_B d_{\text{actin}}^2$ [25], where d_{actin} is the interactin distance and ℓ_B is the Bjerrum length. For the mesh of DNA, the solution's osmotic pressure is $\Pi_{\text{DNA}} \propto k_B T/\ell_B \xi_{\text{DNA}}^2 \propto k_B T \rho_{\text{DNA}}/\ell_B$. To find the equilibrium density of the F-actin
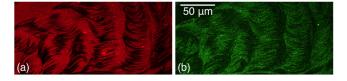
FIG. 4 (color online). Fluorescence confocal image of DNA F-actin mixture at 5 mM KCl ([DNA]/[G-actin] = 13). (a) DNA [gray (red)] infiltrates into the elongated (b) F-actin [gray (green)] domains and breaks them up into smaller F-actin subdomains surrounded by DNA.

rods and the average spacing between them in this strongly charged counterion-controlled regime, we use the mechanical balance between the nematic actin domain and the surrounding DNA solution. From the pressure balance $\Pi_{DNA} = \Pi_{actin}$, one recovers the experimentally observed power-law dependence $d_{actin} \propto \rho_{DNA}^{-1/2}$. In agreement with experiments, this dependence holds for different contour lengths of DNA, as long as they are $> \lambda_{DNA}$.

As monovalent salt is added to the system, the behavior should approach that for a system of polymers with depletion interactions [26] [Figs. 3(f) and 3(g)]. The osmotic pressure of a one-component polyelectrolyte solution changes from a counterion-dominated regime with no added salt to a significantly weaker polymer depletion regime with low concentrations of added monovalent salt (<10 mM) [24]. With increasing monovalent salt, the nematic correlation peaks are progressively suppressed, with reduced amplitudes and increased peak widths, indicating that the average domain sizes have sharply decreased. All nematic correlation peaks eventually disappear as salt is added [Fig. 3(f)]. Moreover, with added salt, the actin interaxial spacing d exhibits a different functional form with a much weaker dependence on [DNA]/[G-actin], which we approximate with a power law with exponent -0.20 ± 0.05 [Fig. 3(g)]. In a DNA/ F-actin mixture at 5 mM KCl, confocal microscopy shows that DNA infiltrates into the elongated F-actin domains (Fig. 4), thereby reorganizing them into "comblike" structures with smaller F-actin subdomains surrounded by DNA, suggestive of conventional depletion. The two mechanisms with different functional forms, which are both entropic in origin, stabilize actin domains of different sizes. These results show that a strongly charged rod-coil polymer system behaves differently from other rod-coil systems with conventional depletion, and can be exquisitely responsive to salt conditions.

*Ivan.Smalyukh@colorado.edu
†gclwong@illinois.edu

[1] P. M. Chaikin and T. C. Lubensky, *Principles of Condensed Matter Physics* (Cambridge University Press, Cambridge, England, 1995).

[2] W. R. K. A. Ciferri and R. B. Meyer, *Polymer Liquid Crystals* (Academic, New York, 1982).

[3] B. Vigolo, A. Pénicaud, C. Coulon, C. Sauder, R. Pailler, C. Journet, P. Bernier, and P. Poulin, Science **290**, 1331 (2000).

[4] P. N. Prasad, *Nanophotonics* (Wiley, New York, 2004).

[5] D. J. Fishkind and Y. Wang, J. Cell Biol. **123**, 837 (1993).

[6] K. Katoh, K. Hammar, P. J. S. Smith, and R. Oldenbourg, Mol. Biol. Cell **10**, 197 (1999).

[7] F. Vollrath and D. P. Knight, Nature (London) **410**, 541 (2001).

[8] G. Zanchetta, M. Nakata, M. Buscaglia, T. Bellini, and N. A. Clark, Proc. Natl. Acad. Sci. U.S.A. **105**, 1111 (2008).

[9] P. J. Flory, Macromolecules **11**, 1138 (1978).

[10] R. de Vries, Biophys. J. **80**, 1186 (2001).

[11] X. Li and M. M. Denn, Macromolecules **35**, 6446 (2002).

[12] G. W. Adams and J. M. G. Cowie, Polymer **40**, 1993 (1999).

[13] O. V. Zribi, H. Kyung, R. Golestanian, T. Liverpool, and G. C. L. Wong, Europhys. Lett. **70**, 541 (2005).

[14] O. V. Zribi, H. Kyung, R. Golestanian, T. B. Liverpool, and G. C. L. Wong, Phys. Rev. E **73**, 031911 (2006).

[15] Z. Dogic, J. Zhang, A. W. C. Lau, H. Aranda-Espinoza, P. Dalhaimer, D. E. Discher, P. A. Janmey, R. D. Kamien, T. C. Lubensky, and A. G. Yodh, Phys. Rev. Lett. **92**, 125503 (2004).

[16] M. Nakata, G. Zanchetta, B. D. Chapman, C. D. Jones, J. O. Cross, R. Pindak, T. Bellini, and N. A. Clark, Science **318**, 1276 (2007).

[17] L. Onsager, Ann. N.Y. Acad. Sci. **51**, 627 (1949).

[18] See EPAPS Document No. E-PRLTAO-101-057846 for an animation showing the 3D network of F-actin domains. For more information on EPAPS, see http://www.aip.org/ pubservs/epaps.html.

[19] V. G. Taratuta, F. Lonberg, and R. B. Meyer, Phys. Rev. A **37**, 1831 (1988).

[20] T. Odijk, Macromolecules **19**, 2313 (1986).

[21] A. Suzuki, T. Maeda, and T. Ito, Biophys. J. **59**, 25 (1991).

[22] F. Oosawa, *Polyelectrolytes* (Marcel Dekker, New York, 1971).

[23] L. Wang and V. A. Bloomfield, Macromolecules **24**, 5791 (1991).

[24] E. Raspaud, M. da Conceicao, and F. Livolant, Phys. Rev. Lett. **84**, 2533 (2000).

[25] Note that only uncondensed counterions contribute to the osmotic pressure since condensed counterions do not carry significant translational entropy. In the theory of counterion condensation, the uncondensed counterions are determined by the effective charge density $1/\ell_B$.

[26] R. Verma, J. C. Crocker, T. C. Lubensky, and A. G. Yodh, Phys. Rev. Lett. **81**, 4004 (1998).